Journal of Applied Electrochemistry **30**: 1405–1413, 2000.

Study of cerium species in molten Li_2CO_3–Na_2CO_3 in the conditions used in molten carbonate fuel cells. Part I: Thermodynamic, chemical and surface properties[†]

V. CHAUVAUT[1], V. ALBIN[1], H. SCHNEIDER[1], M. CASSIR[1]*, H. ARDÉLÉAN[2] and A. GALTAYRIES[2]
[1]*Ecole Nationale Supérieure de Chimie de Paris, Laboratoire d'Electrochimie et de Chimie Analytique (UMR 7575 du CNRS), 11 rue Pierre et Marie Curie, 75231 Paris Cedex 05, France*
[2]*Ecole Nationale Supérieure de Chimie de Paris, Laboratoire de Physicochimie des Surfaces Métalliques (UPRESA 7045 du CNRS)*
*(*author for correspondence, fax: (+33) 1 44 27 67 50, e-mail: cassir@ext.jussieu.fr)*

Received 31 July 1999; accepted in revised form 11 January 2000

Key words: cerium, lithium, molten carbonate, potential–acidity diagrams, sodium, solubility, thermodynamics

Abstract

The chemical and surface behaviour of cerium oxide, a candidate material for MCFC applications is analysed in Li_2CO_3–Na_2CO_3 carbonate eutectic in reducing (H_2:CO_2:H_2O:CO) and oxidizing (O_2:CO_2) atmospheres. The electrochemical stability domains of cerium species are established at different temperature on the basis of thermochemical calculations. CeO_2 is the stable species whatever the acidity level in both the anode and cathode conditions; nevertheless, a partial solubility of Ce_2O_3 in CeO_2 can be predicted. The solubility of cerium and cerium oxide samples, determined by absorption spectrophotometry, is about 5×10^{-4} mol kg^{-1} in cathodic conditions and 3×10^{-4} mol kg^{-1} in anodic conditions. X-ray diffraction (XRD) confirmed the presence of CeO_2 at the surface of the samples. Incorporation of sodium species in the CeO_2 lattice is likely; the presence of Ce(III) in long endurance tests was detected by X-ray photoelectron spectroscopy (XPS).

1. Introduction

One of the principal challenges in the quest to improve the lifetime and performance of molten carbonate fuel cells (MCFC) is the control of solubility and corrosion processes occurring in the electrode–electrolyte interfaces, in particular at the cathode, and in the bipolar plate contact areas. Other problems concern the nature of the molten carbonate electrolyte (corrosiveness, evaporation etc.) and the inertness and properties of the solid support (i.e., $LiAlO_2$). Thus, it is of a great interest to find new materials to improve or replace the present anode (Ni + Cr) and cathode ($Li_xNi_{1-x}O$) as well as to protect the stainless steels used as bipolar plates.

Although very few data exist on the behaviour of cerium species in molten carbonate, the use of cerium oxide has been mentioned in the literature, as an alternative anode (doped CeO_2), bipolar plate coating or inert support for the electrolyte [1–4]. CeO_2 pellets were used as indirect way of gauging the oxygen activity in molten Li_2CO_3–K_2CO_3 by observing microstructural changes in CeO_2 after molten carbonate exposure; the presence of $Ce_{11}O_{20}$ and Ce_6O_{11} was identified by XRD [5]. A double-layered cathode with lithiated nickel oxide and cerium activated cobaltite has been described in a recent patent [6]. CeO_2 has a cubic fluorite structure and is an insulator at room temperatures. This compound deviates strongly from its stoichiometric composition at elevated temperature. This oxygen deficient oxide, CeO_{2-x}, may be classified as a n-type semiconductor, with a value of x around $10^{-4} - 10^{-5}$ under oxidising conditions and a temperature range between 700–1000 °C [7, 8]. Its conductivity can be increased by addition of dopants [9]. The protective role of cerium oxide coatings is often described in the literature. A thorough study has been realised on CeO_2 deposits by electrophoresis on a ferritic steel without nickel, Z2CT17 [10]. Very efficient coatings improved the corrosion resistance in thermal cycling conditions from 25 to 950 °C: no spalling was observed for assays of 40 cycles spread over more than five days. Reversible lithium insertion has been noted in CeO_2 coatings produced by the sol–gel process [11]. A decrease in the oxidation rate of nickel covered by CeO_2 has been observed [12]. Other substrates have been used with the same favourable effect, Y_2O_3-doped cerium [13] and Gd_2O_3-doped cerium [14]. Apart from the sol-gel procedure, other coating techniques have been performed: electrochemical vapour deposition [13], or

[†] Dedicated to the memory of Daniel Simonsson

liquid deposition [14]. Roure et al. [15] have shown that the presence of CeO_2 at the surface of chromium (one of the components of stainless steels used as MCFC bipolar plates) decreases its oxidation rate and improves the adhesion of the Cr_2O_3 layer at the metal surface. CeO_2 coatings have also been deposited to protect the high-aluminium content 800H stainless steel [16].

The aim of this work is to analyse the general behaviour of cerium oxide and metallic cerium in the most probable second-generation MCFC electrolyte, Li_2CO_3–Na_2CO_3 eutectic, at 650 °C. As a first step, the thermodynamic stability of cerium species is deduced from potential–acidity diagrams based on available thermochemical data, in the usual equilibrium conditions of the anode ($H_2 + CO_2$, 80:20, humidified with water heated at 60 °C) and cathode (Air + CO_2, 70:30). Different experiments are carried out to verify these thermodynamic predictions. The solubility of cerium is determined in both anode and cathode conditions at 650 °C. The surface characterisation of cerium oxide samples is given by X-ray diffraction (XRD) and X-ray photoelectron spectroscopy (XPS). A second paper is dedicated to the electrochemical behaviour of cerium species [17].

2. Thermodynamic predictions

The general properties and electrochemical stability domains of alkali molten carbonate have been fully analysed in previous papers, describing, in particular, the stability of oxygen species [18, 19], nickel [20, 21] and titanium [22] compounds. All the potentials calculated are referred to Li_2O/O_2 system (Li_2O being more stable than Na_2O in the mentioned eutectic) with $a(Li_2O) = 1$ and $P(O_2) = 1$ atm, with a standard potential $E^*(O_2/Li_2O) = 0$ V. As more details are given in other studies [19, 22], it is unnecessary to reintroduce them in the present one.

2.1. *Anodic conditions*

The cerium species which may exist in the melt in anodic conditions are as follows: cerium hydroxides, alkali and cerium mixed oxides, Ce_2O_3, CeO_2, cerium hydride and carbides. Very few data are available in the literature concerning cerium in nonaqueous conditions. As no data were found concerning cerium carbonates, hydroxides and mixed oxides, these compounds were not considered in the establishment of oxoacidity–potential diagrams. Only the following species are listed in thermochemical tables: CeC_2, Ce_2C_3, CeH_2, Ce, Ce_2O_3, CeO_2. Standard potentials of the different redox reactions were calculated from the free enthalpies of the corresponding chemical reactions.

As few cerium species are described thermodynamically in the literature, all the principal chemical equilibria were represented taking into account that, in the absence of oxygen, H_2O is the best oxidizing agent (with stronger oxidizing properties than CO_2). These equilibria are summarised in a synthetic form (where x, y, z and t are general stoichiometric coefficients):

$$2\ CeC_2 + 2\ H_2O \Leftrightarrow Ce_2C_3 + CO_2 + 2\ H_2 \quad (1)$$

$$Ce_xC_y + 2yH_2O \Leftrightarrow xCeH_2 + yCO_2 + (2y - x)H_2 \quad (2)$$

$$Ce_xC_y + (xt + 2yz)H_2O \Leftrightarrow xCe_zO_t + yzCO_2 + (xt + 2yz)H_2 \quad (3)$$

$$xCeH_2 + yH_2O \Leftrightarrow Ce_xO_y + (x + y)H_2 \quad (4)$$

$$zCe_xO_y + (xt - yz)H_2O \Leftrightarrow Ce_zO_t + (xt - yz)H_2 \quad (5)$$

The standard free enthalpies of these reactions are obtained, using the relation: $\Delta_rG^\circ = \Sigma_i v_i \Delta_fG_i^\circ$, where Δ_rG° represents the free enthalpy of reaction, $\Delta_fG_i^\circ$ and v_i represent, respectively, the free enthalpy of the species i and its stoechiometric coefficient in the reaction. Standard formation values were calculated at 550, 650 and 750 °C, using the van't Hoff relation, assuming that the standard enthalpies and entropies are independent of temperature:

$$\frac{d(\Delta_rG^\circ/T)}{dT} = -\frac{\Delta_rH^\circ}{T^2} \Rightarrow \Delta_rG^\circ(T_2) = \Delta_rG^\circ(T_1) \times \frac{T_2}{T_1} + \Delta_rH^\circ\left(1 - \frac{T_2}{T_1}\right).$$

The corresponding redox reactions involving cerium species, for which free enthalpies of formation are known, are described here:

$$2\ CeC_2 + 2\ H_2O + 2\ O^{2-} \rightarrow Ce_2C_3 + CO_2 + H_2 + O_2 + 4\ e^- \quad (6)$$

$$Ce_xC_y + 2\ H_2O + 2yO^{2-} \rightarrow xCeH_2 + yCO_2 + (2y - x)H_2 + yO_2 + 4ye^- \quad (7)$$

$$zCe_xC_y + (xt + 2yz)H_2O + (xt + yz)O^{2-} \rightarrow xCe_zO_t + yzCO_2 + (xt + 2yz)H_2 + \frac{xt + 2yz}{2}O_2 + 2(xt + 2yz)e^- \quad (8)$$

$$xCeH_2 + yH_2O + yO^- \rightarrow Ce_xO_y + (x + y)H_2 + \frac{y}{2}O_2 + 2ye^- \quad (9)$$

$$zCe_xO_y + (xt - yz)H_2O + (xt - yz)O^- \rightarrow xCe_zO_t + (xt - yz)H_2 + \frac{xt - yz}{2}O_2 + 2(xt - yz)e^- \quad (10)$$

The values of the standard potentials in anodic conditions are reported in Table 1. Nernst equations as a

Table 1. Values of the standard potentials of cerium redox systems in anodic conditions

Systems	$E°$/V 550 °C	$E°$/V 650 °C	$E°$/V 750 °C
CeC_2/Ce_2C_3	−0.127	−0.157	−0.188
CeC_2/CeH_2	0.010	0.002	−0.007
CeC_2/Ce	0.113	0.086	0.059
CeC_2/Ce_2O_3	−0.367	−0.382	−0.391
CeC_2/CeO_2	−0.367	−0.377	−0.387
Ce_2C_3/CeH_2	0.078	0.081	0.084
Ce_2C_3/Ce	0.193	0.167	0.141
Ce_2C_3/Ce_2O_3	−0.421	−0.431	−0.436
Ce_2C_3/CeO_2	−0.415	−0.421	−0.427
CeH_2/Ce	0.423	0.340	0.256
CeH_2/Ce_2O_3	−0.820	−0.841	−0.852
CeH_2/CeO_2	−0.747	−0.755	−0.767
Ce/Ce_2O_3	−1.648	−1.629	−1.590
Ce/CeO_2	−1.327	−1.302	−1.278
Ce_2O_3/CeO_2	−0.364	−0.322	−0.344

function of the activities of the compounds involved in the reactions, CO_2, CO, H_2O and H_2 partial pressures are as follows:

$$E_6 = E_6^\circ + \frac{\Delta_f G^\circ(H_2O)}{2F} + \frac{2.3\,RT}{4F}\left(2pK_d^* - 3pCO_2\right) + \frac{2.3\,RT}{4F}\log\left(\frac{a(Ce_2C_3)}{a^2(CeC_2)}\right)$$

$$E_7 = E_7^\circ + \frac{\Delta_f G^\circ(H_2O)}{2F} + \frac{2.3\,RT}{4F}\left(2pK_d^* - 3pCO_2\right) + \frac{2.3\,RT}{4yF}\log\left(\frac{a^x(CeH_2)}{a(Ce_xC_y)\times P^x(CO_2)}\right)$$

$$E_8 = E_8^\circ + \frac{\Delta_f G^\circ(H_2O)}{2F} + \frac{2.3\,RT}{2(xt+2yz)F} \times \left[(xt+2yz)pK_d^* - (2xt+3yz)pCO_2\right] + \frac{2.3\,RT}{2(xt+2yz)F}\log\frac{a^x(Ce_zO_t)}{a^z(Ce_xC_y)}$$

$$E_9 = E_9^\circ + \frac{\Delta_f G^\circ(H_2O)}{2F} + \frac{2.3\,RT}{2F}(pK_d^* - pCO_2) + \frac{2.3\,RT}{2yF}\log\frac{a(Ce_xO_y)\times P^x(H_2)}{a^x(CeH_2)}$$

$$E_{10} = E_{10}^\circ + \frac{\Delta_f G^\circ(H_2O)}{2F} + \frac{2.3\,RT}{2F}(pK_d^* - pCO_2) + \frac{2.3\,RT}{2(xt-yz)F}\log\frac{a^x(Ce_zO_t)}{a^z(Ce_xO_y)}$$

knowing that $pCO_2 = -\log(P_{CO_2})$ and that the values of the partial pressures of water and hydrogen are those used in the standard anodic MCFC conditions.

2.2. *Cathodic conditions*

The cathodic conditions are defined by a mixture of air/CO_2, the stronger oxidising agent being molecular oxygen. The compounds formed in such conditions are the same as on the anodic side, except that cerium hydride cannot exist. The chemical equilibria can be expressed in a synthetic way by the following:

$$2\,CeC_2 + O_2 \leftrightarrow Ce_2C_3 + CO_2 \tag{11}$$

$$zCe_xC_y + \left(\frac{xt}{2} + yz\right)O_2 \leftrightarrow xCe_zO_t + yzCO_2 \tag{12}$$

$$zCe_xO_y + \frac{xt-yz}{2}O_2 \leftrightarrow xCe_zO_t \tag{13}$$

The corresponding redox reactions are as follows:

$$2\,CeC_2 + 2\,O^{2-} \rightarrow Ce_2C_3 + CO_2 + 4\,e^- \tag{14}$$

$$zCe_xC_y + (xt+2yz)O^{2-} \rightarrow xCe_zO_t + yzCO_2 + 2(xt+2yz)e^- \tag{15}$$

$$zCe_xO_y + (xt-yz)O^- \rightarrow xCe_zO_t + 2(xt-yz)e^- \tag{16}$$

The values of the standard potentials in cathodic conditions are reported in Table 2. Nernst equations as a function of the activities of the compounds involved in the reactions and carbon dioxide partial pressure are the following:

$$E_{14} = E_{14}^\circ + \frac{2.3\,RT}{4F}(2pK_d^* - 3pCO_2) + \frac{2.3\,RT}{4F}\log\frac{a(Ce_2C_3)}{a^2(CeC_2)}$$

$$E_{15} = E_{15}^\circ + \frac{2.3\,RT}{2(xt+2yz)F} \times \left[(xt+2yz)pK_d^* - (xt+3yz)pCO_2\right] + \frac{2.3\,RT}{2(xt+2yz)F}\log\frac{a^x(Ce_zO_t)}{a^z(Ce_xC_y)}$$

$$E_{16} = E_{16}^\circ + \frac{2.3\,RT}{2F}(pK_d^* - pCO_2) + \frac{2.3\,RT}{2(xt-yz)F}\log\frac{a^x(Ce_zO_t)}{a^z(Ce_xO_y)}$$

Table 2. Values of the standard potentials of cerium redox systems in cathodic conditions

Systems	$E°$/V 550 °C	$E°$/V 650 °C	$E°$/V 750 °C
CeC_2/Ce_2C_3	−1.187	−1.177	−1.179
CeC_2/Ce	−0.947	−1.106	−0.932
CeC_2/Ce_2O_3	−1.427	−1.402	−1.382
CeC_2/CeO_2	−1.427	−1.397	−1.378
Ce_2C_3/Ce	−0.867	−0.853	−0.850
Ce_2C_3/Ce_2O_3	−1.481	−1.451	−1.427
Ce_2C_3/CeO_2	−1.475	−1.441	−1.418
Ce/Ce_2O_3	−2.708	−2.649	−2.581
Ce/CeO_2	−2.387	−2.322	−2.269
Ce_2O_3/CeO_2	−1.424	−1.342	−1.335

2.3. *Potential–acidity diagrams*

All cerium species are in solid form at the selected temperatures. As a first approximation, all the solids were considered totally unmixed. Therefore, the activities of cerium species are equal to 1. Potential–acidity diagrams, representing Nernst equations in both anodic and cathodic conditions, were established at three temperatures, 550, 650 and 750 °C. In all the cases, CeO_2 is the only stable species of cerium. Moreover, in the anodic conditions, metallic cerium disproportionates into hydride and Ce_2O_3, species which are not stable and are transformed in CeO_2. An example is given under anodic atmosphere at 650 °C in Figure 1. The basic limit is constituted by the melt saturated by Li_2O and the acidic limit by carbon dioxide vapour pressure, set arbitrarily at one atmosphere. The oxidation limit is due to molecular oxygen in acidic and neutral media and peroxide species in basic media (with an activity of 10^{-3}). The reduction limit is due to the formation of sodium in basic media and to the reduction of water or carbon dioxide in acidic media.

2.4. *Species partially mixed with CeO_2*

The activity at which other cerium species could possibly be formed in the melt when partially mixed with CeO_2 was determined. The formation of these compounds from CeO_2 was considered and the activity corresponding to their stabilization in the melt calculated. In the case of the metallic cerium, hydrides and carbides, the highest activity is about 10^{-6}; therefore, their presence in the melt in unlikely. In the case of Ce_2O_3, the formation reactions in anodic and cathodic conditions are the following:

$$2\,CeO_2 + H_2 \leftrightarrow Ce_2O_3 + H_2O \qquad (17)$$

$$2\,CeO_2 \leftrightarrow Ce_2O_3 + \tfrac{1}{2}O_2 \qquad (18)$$

Equilibrium constants of these reactions were calculated and the activity of Ce_2O_3 deduced, using the partial pressures relative to the anodic and cathodic conditions. The results are presented in Table 3. It can be concluded that even though CeO_2 is thermodynamically stable, the presence of Ce(III), in the form of Ce_2O_3, may occur to a minor degree under anodic conditions. A very small stability domain of this Ce(III) species in moderately basic media can be observed in Figure 1.

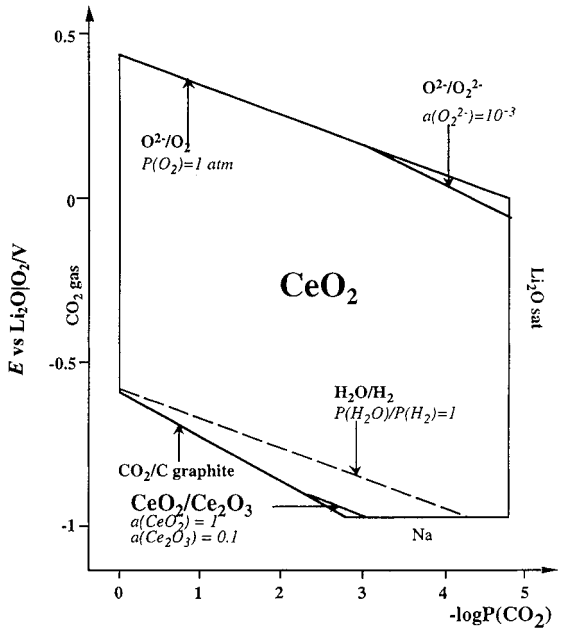

Fig. 1. Potential–acidity diagram of cerium in Li_2CO_3–Na_2CO_3 eutectic at 650 °C under anodic atmosphere: $H_2 + CO_2$, 80:20, humidified with water heated at 60 °C.

3. Experimental details

Lithium and sodium carbonates, mixed in proportions of 52–48 mol %, were Merck reagents of analytical purity (>98%). The carbonates were previously stored in a dry atmosphere. The standard cathodic and anodic atmosphere were fully described in previous papers [20, 21].

The cell with the carbonate melt was a compact single-compartment crucible 70×50 mm^2 (Degussa Al 23) contained in another Al 23 250×60 mm^2 crucible hermetically closed by a stainless steel cover with a Viton O-ring. The reference electrode and the auxiliary electrodes were fully described elsewhere [20]. The samples, which constituted the working electrodes, were either metallic cerium rods of 7×40 mm^2 or cerium foils $10 \times 10 \times 0.25$ mm^3 (Goodfellow, 99.9% purity) handled by a gold wire (1 mm dia.), or cerium oxide pellets of 12×4 mm^2, with 99.9% purity grade, provided by Cerac. Temperature control was achieved with a West 3810 Gulton regulator and a calibrated chromel–alumina thermocouple.

Each sample was introduced into the electrochemical cell, and exposed for 36 h to the gaseous atmosphere above the melt (time necessary for reaching gas equilibrium) and subsequently immersed in the molten carbon-

Table 3. Free enthalpies of Reactions 17 and 18 and values of the activity of Ce_2O_3 in CeO_2

Gas	Anodic			Cathodic		
T/°C	550	650	750	550	650	750
$\Delta G°$/kJ mol^{-1}	70.202	66.34	62.202	272.463	259.030	257.659
$a(Ce_2O_3)$	1.1×10^{-4}	6.0×10^{-4}	2.27×10^{-3}	3×10^{-17}	1.5×10^{-14}	5×10^{-13}

ate for more than 48 h (until, for all the cerium samples, the measured open-circuit potential became stationary). Then, the sample was removed from the molten mixture, air-cooled and rinsed with de-ionized water before being analysed by XRD and XPS. XRD experiments were carried out with a Siemens CGR type Thêta 60 diffractometer using a Co $K_\alpha 1$ radiation ($\lambda = 1.789$ Å).

XPS measurements were performed with a VG Escalab Mark II spectrometer using the Mg K_α X-ray source ($h\nu = 1253.6$ eV). The spectrometer was calibrated using the reference energies of Au $4f_{7/2}$ (83.8 ± 0.1 eV), and Cu $2p_{3/2}$ (932.7 ± 0.1 eV). A take off angle of 90° was used (angle between the surface and the analyser). A binding energy of 285.0 eV was assigned to the C 1s peak corresponding to the surface contamination and this was used as an internal reference for correction of charging effects.

3.1. *Solubility measurements*

Chemical reagents, of analytical purity (>99%), used for the absorption titration of cerium in the melt were commercialised by Prolabo (silver sulfate, sodium acetate, phenanthroline) and by Aldrich (ammonium persulfate). Absorption measurements were realised with a Shimadzu UV-160A spectrophotometer.

4. Results and discussion

Solubility tests were carried out by dipping Ce rods or CeO_2 pellets in the melt. The samples were kept 48 h and were withdrawn from the carbonates before solidification. The titration is based on the technique presented by Culkin and Riley with a detection limit of 0.5 ppm [23]. Part of the melt was solubilized in water and acidified at pH 1 to avoid the precipitation of Ce(IV) and Ce(III) hydroxides. Afterwards, ammonium persulfate was added, with the presence of silver sulfate as a catalyst, in order to oxidize all the cerium present in the carbonates. The excess ammonium persulfate was destroyed by heating. After cooling, ferrous phenanthroline (with sodium acetate in order to moderate the acidity of the melt and to avoid its decomposition) was added. Ce(IV) reacts with Fe(II), yielding Ce(III) and Fe(III). Ferrous phenanthroline being red coloured with a coloration disappearing when oxidised, the measurement of the absorption allowed the quantification of cerium dissolved in the melt. Three random samples were extracted from the molten salt for each considered condition. The medium cerium solubility obtained with cerium rods or cerium oxide pellets, in anodic and cathodic conditions, is given in Table 4 and compared to the solubility of Ti, TiO_2 and $Li_xNi_{1-x}O$. The results relative to cerium species show a very weak influence of the experimental conditions. The solubility is similar for metallic cerium or cerium oxide. Even though the solubility is slightly lower in anodic than in cathodic conditions, it can be considered in the same order of magnitude. The solubility of cerium is slightly higher, in cathodic conditions, than that of lithiated nickel oxide and significantly higher, in anodic conditions, than that of titanium oxide, another candidate material for bipolar plate coating [2, 3].

Table 4. Solubility of cerium oxide dipped in molten Li + Na carbonate melt at 650 °C compared to that of Ti, TiO_2 and $Li_xNi_{1-x}O$ in anodic or cathodic conditions

Atmosphere	Cathodic/mol kg^{-1}	Anodic/mol kg^{-1}
CeO_2	$(5.0 \pm 0.1) \times 10^{-4}$	$(3.3 \pm 0.1) \times 10^{-4}$
Ce	$(5.0 \pm 0.1) \times 10^{-4}$	$(3.5 \pm 0.1) \times 10^{-4}$
TiO_2 [2]		2.2×10^{-5}
Ti [2]		2.0×10^{-5}
NiO [21]	1.5×10^{-4}	

4.1. *XRD measurements*

All the samples were analysed before and after exposure to the molten carbonate. Metallic cerium before exposure shows an XRD pattern corresponding to cerium oxide. This is not surprising since this metal is known for being oxidized spontaneously in contact with air. This metal is totally consumed in the melt; it is first transformed into CeO_2 and the layer, being very porous does not play any protective role. Cerium is found in the melt in the form of CeO_2 powder. XRD pattern of CeO_2 before exposure is presented in Figure 2. The samples of CeO_2 after exposure in anodic or cathodic MCFC conditions show the same diffractional diagram as for pure CeO_2. No other structure, such as Ce_2O_3 or $Ce_{11}O_{20}$ and Ce_6O_{11} [5] was observed in any case. These results corroborate the thermodynamic predictions concerning the predominant stability of CeO_2 in all the mentioned conditions.

4.2. *XPS measurements*

The survey spectrum of a CeO_2 sample after exposure to Li_2CO_3–Na_2CO_3 at 650 °C during 21 days is presented in Figure 3. In addition to the core levels corresponding to the presence of O, C, Ce and Na on the surface of the sample (also confirmed by the Auger lines), lithium is not detected. Though it represents a very small amount on the CeO_2 surface, this can be explained by the very low photoionization cross section for this element in these experimental conditions (Mg K_α source): 0.059. This presence may be detected by more sensitive techniques, such as secondary ion mass spectroscopy (SIMS). This spectrum is very close to that obtained after an exposure time of about two days, except that a significant increase in the peak intensity of Na is noted from two to 21 days. The spectra corresponding to Ce 3d, O 1s and C 1s regions are reported respectively in Figures 4–6. In Figure 4, the Ce 3d spectrum may originate from different chemical states. The Ce $3d_{5/2}$ and Ce $3d_{3/2}$ peaks can be well fitted by single peaks corresponding to Ce(IV) and Ce(III). The Ce 3d

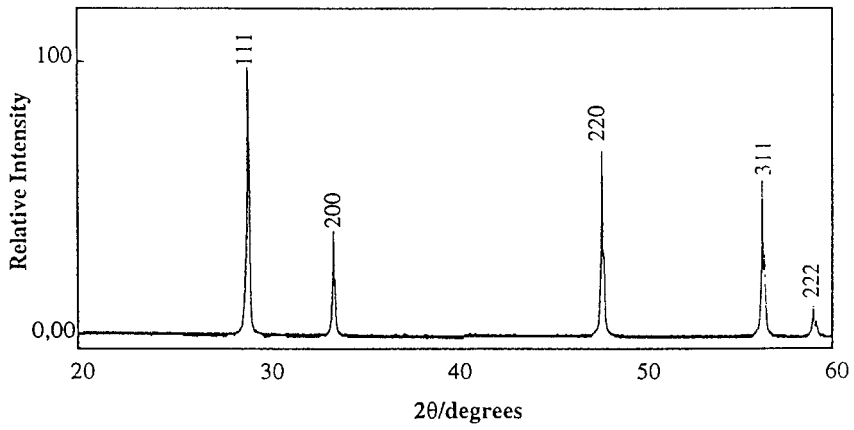

Fig. 2. XRD pattern of a CeO_2 pellet using a Co $K_\alpha 1$ radiation ($\lambda = 1.789$ Å).

spectroscopy is complex owing to a satellite structure and hybridization problems and it is not our purpose to give a detailed analysis of the resolution of Ce 3d spectrum; various authors have described the structures v_0, v, v', v'', v''', u_0, u, u', u'' and u''' [24–26]. Table 5 gives a summary of the initial and final spectroscopic states of Ce^{4+} and Ce^{3+} for Ce 3d spectrum. An estimation of $C_{Ce^{3+}}$, the concentration of Ce^{3+}, can be calculated from the following relation [27]:

$$C_{Ce^{3+}} = \frac{(v_0 + v' + u_0 + u')}{(v_0 + v + v' + v'' + v''' + u_0 + u + u' + u'' + u''')} \quad (19)$$

According to this formula and after peak decomposition, the Ce 3d region indicates a proportion of about 75% of Ce^{4+} with respect to the total amount of this species. The presence of 25% of Ce^{3+}, could result from different causes: (i) the exposure to X-rays in the spectrometer inducing a surface reduction of Ce^{4+} in Ce^{3+} [27], (ii) the formation of Ce_2O_3 in the conditions of the molten carbonate eutectic, or (iii) the formation of $MCeO_2$ compound at the surface of the electrode. The first cause is probably the most important one according to different studies reporting the XPS behaviour of CeO_2 [24, 27]. Nevertheless, a moderate presence of Ce(III) at the electrode in the MCFC conditions can be predicted.

The O 1s spectrum of Figure 4 may be decomposed into four features: a principal peak at low binding energies, ascribed to O^{2-}, characteristic of a O–Ce bond (most probably CeO_2 or Ce_2O_3). The second peak corresponds to adsorbed carbonates CO_3(ads), the

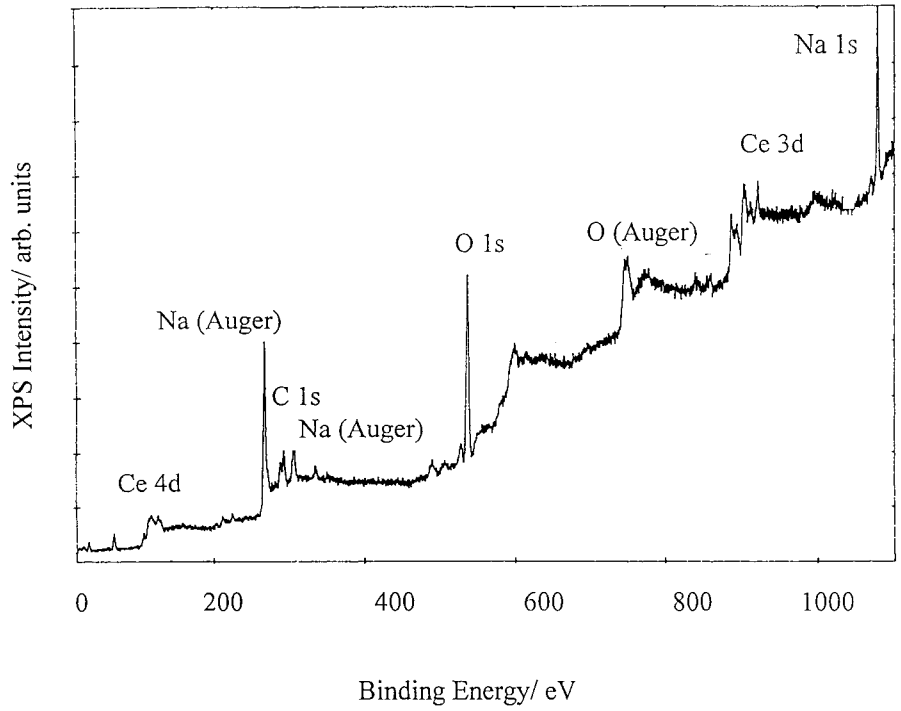

Fig. 3. XPS survey spectrum of a CeO_2 pellet after exposure during 21 days in Li_2CO_3–Na_2CO_3 under anodic atmosphere: $H_2 + CO_2$, 80:20, humidified with water heated at 60 °C.

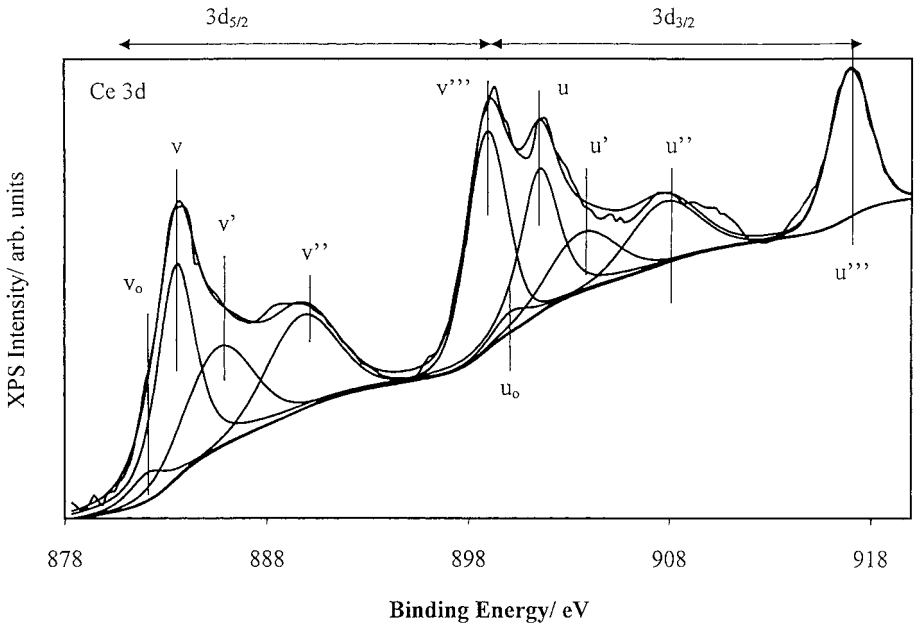

Fig. 4. XPS spectrum of Ce $3d_{5/2}$ and $3d_{3/2}$, relative to a CeO_2 pellet after exposure during 21 days in Li_2CO_3–Na_2CO_3 under anodic atmosphere: $H_2 + CO_2$, 80:20, humidified with water heated at 60 °C.

intense peak to adsorbed hydroxide OH(ads) and the small shoulder at higher energies to adsorbed molecules of water H_2O(ads). Figure 6 shows the high resolution spectrum of C 1s. It reveals two peaks, one due to adsorbed carbonates and another to surface contaminations, that is, carbon present in the analysis room at 285 eV (deducing 6.4 eV due to charging effect).

To determine the proportion of the different species present in the superficial layer of CeO_2, a semiquantitative analysis was carried out based on the ratio of the atomic densities of species A and B in the sample per surface unit:

$$\frac{D_A}{D_B} = \frac{I_A}{I_B}\frac{\lambda_B}{\lambda_A}\frac{T_B}{T_A}\frac{\sigma_B}{\sigma_A} \tag{20}$$

With I, the intensity of the signal emitted by elements A or B in a solid of infinite thickness (peak areas in counts per second); λ, the inelastic mean path [28]; T, transmission function of the analyser [29] and σ, the Hartree–Slater subshell photoionization cross-section for Mg K_α [30]. Table 6 shows values of the binding energies (B.E.) of Ce, O, C, Na and Li with the respective values of σ. In our experimental conditions, a simplified formula was used [31]:

$$\frac{D_A}{D_B} = \frac{I_A}{I_B}\left(\frac{E_k^A}{E_k^B}\right)^{-0.16}\frac{\sigma_B}{\sigma_A} \tag{21}$$

with $E_k = h\nu - \phi$, where E_k is the kinetic energy of the emitted electron, and ϕ, the work function of the spectrometer (4 eV).

Table 7 shows the ratio of the atomic densities for different pairs of species. A few observations can be made:

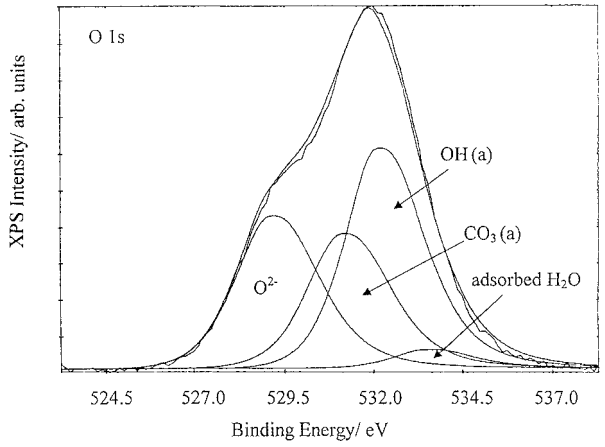

Fig. 5. XPS spectrum of O 1s, relative to a CeO_2 pellet after exposure during 21 days in Li_2CO_3–Na_2CO_3 under anodic atmosphere: $H_2 + CO_2$, 80:20, humidified with water heated at 60 °C.

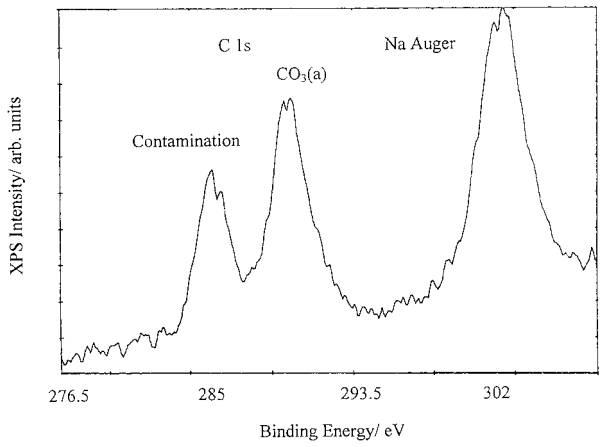

Fig. 6. XPS spectrum of C 1s, relative to a CeO_2 pellet after exposure during 21 days in Li_2CO_3–Na_2CO_3 under anodic atmosphere: $H_2 + CO_2$, 80:20, humidified with water heated at 60 °C.

Table 5. Initial and final states of Ce^{4+} and Ce^{3+} ions of Ce 3d level and description of the different peaks

Ion	Initial state	Final state	Ce $3d_{5/2}$ and Ce $3d_{3/2}$ peaks
Ce^{4+}	$3d^{10}4f^0$	$3d^94f^2V^{n-2}$	v, u
Ce^{4+}	$3d^{10}4f^0$	$3d^94f^1V^{n-1}$	v'', u''
Ce^{4+}	$3d^{10}4f^0$	$3d^94f^0V^n$	v''', u'''
Ce^{3+}	$3d^{10}4f^1$	$3d^94f^2V^{n-1}$	v_0, u_0
Ce^{3+}	$3d^{10}4f^1$	$3d^94f^1V^n$	v', u'

Table 6. Values of the binding energies (B.E.) for Ce 3d, O 1s, C 1s, Na 1s and Li 1s peaks with their respective σ, photoionization cross-section for Mg K_α [28]

	Ce $3d_{5/2}$	Ce $3d_{3/2}$	Ce $4d_{5/2}$	Ce $4d_{3/2}$	O 1s	C 1s	Na 1s	Li 1s
B.E. /eV	882	900	108	112	531	285	1072	56
σ	19.67	28.57	3.74	2.58	2.85	1.00	7.99	0.059

(a) After peak decomposition of O 1s and C 1s core levels, we have checked the $D_{O/(\underline{CO}_3)}/D_{C/(\underline{CO}_3)}$ which is equal to 2.7. This is rather satisfying compared to the expected value of 3, within the error margin.

(b) So, from this decomposition, we have looked for the amount of sodium carbonates. If sodium was totally in the carbonate form (with the composition of Li_2CO_3–Na_2CO_3 52–48 mol %), the expected theoretical $D_{Na}/D_{\underline{CO}_3}$ ratio would be around unity. We have obtained 1.67 which indicates that not all the sodium is bound to carbonates. Another possibility is that sodium cations are inserted in the ceria lattice to form a mixed oxide compound. This also agrees with the fact that $D_{Na}/D_{\underline{CO}_3}$ increases with exposure time to the melt.

(c) The D_{Ce3d}/D_{Ce4d} which is correlated to the homogeneity of the sample surface (as the mean free paths are completely different in the Ce 3d or Ce 4d core levels) is lower than 1. The 0.83 value obtained here tends to signify that in addition to the ceria bulk, there is a layer on its surface probably composed of carbonates, hydroxides and adsorbed water.

(d) The fact that sodium oxide does not precipitate in the experimental conditions of the melt, seems to dismiss the detection of sodium oxide. A small amount of sodium hydroxide after rinsing the sample may be formed.

(e) As already mentioned a small amount of Ce(III) may be present at the surface of the sample after exposure to the carbonate melt.

Table 7. Ratios of the atomic densities of different species A and B in the case of CeO_2 sample after exposure to Li_2CO_3–Na_2CO_3 at 650 °C during 21 days, under anodic atmosphere: H_2 + CO_2, 80:20, humidified with water heated at 60 °C

D_A/D_B	Na/Ce_{ttotal}	Na/CO_3	$O(CO_3)/C(CO_3)$	Ce 3d/Ce 4d
Ratio	2.7	1.65 (1.41*)	2.7	0.83

* Exposure time of 2 days

5. Conclusion

According to thermochemical predictions, the stable species of cerium in the anodic and cathodic conditions used in MCFC is CeO_2. Nevertheless, at potentials close to the reduction limit of the electrochemical stability domain, and considering a partial solubility of Ce_2O_3 in CeO_2, it is possible to form a Ce(III) species. It was impossible to predict the theoretical dissolution of CeO_2 at MCFC working temperatures because of the lack of thermochemical data. The experimental solubility of cerium, measured by spectrophotometry was around 4×10^{-4} mol kg^{-1} in oxidizing and reducing conditions (slightly lower in the second case). The presence of CeO_2 was detected by XRD in layers of about 1 μm. In very thin layers of about 50 Å, the situation is more complex. A semiquantitative analysis showed that both Ce(IV) and Ce(III) species can be present. Ce(III) was mostly formed by the exposure to X-rays in the spectrometer inducing a surface reduction of Ce^{4+} in Ce^{3+}, but a certain amount could originate from the formation of Ce_2O_3 or/and $MCeO_2$ compounds at the surface of the electrode in contact with the molten carbonate. The existence of a certain amount of sodium at the surface of CeO_2 is in accordance with the formation of a compound with cerium, $NaCeO_2$, or its incorporation in the CeO_2 lattice, Na_xCeO_2.

Acknowledgements

The authors thank Gaz de France (GDF/CNRS/ENSCP 414) and the European Community (Joule N°JOE3-CT950024) for financial and support. Thanks are also due to Dr B. Malinowska, A. Alfarra and J.M. Sifre.

References

1. C. Yuh, R. Johnsen, M. Farooque and H. Maru, *J. Power Sources* **56** (1995) 1.
2. V. Chauvaut, PhD thesis, University of Paris VI (ENSCP), France (1998).
3. M. Keijzer, K. Hemmes, P.J.J.M. van der Put, J.H.W. De Wit and J. Schooman, *Corros. Sci.* **39** (1997) 483.
4. K. Myles, M. Krumpelt, G. Kucera, M. Roche and E. Indacochea, Proceedings of the Joint Contractors Meeting: Conference on 'Advanced Turbine Systems, Fuel Cells and Coal-Fired Heat Engines' Morgantown, WV, USA, 3–5 Aug. (1993), p. 386.
5. E. Dincer-Cubukcu and M.R. DeGuire, *Mater. Lett.* **10** (1991) 379.
6. A. Prohasha, B. Rohland, M. Bischoff and V. Plzak, *WO 98/53513 Int. Patent* (1998).
7. J.R. Sims and R.N. Blumenthal, *High Temp. Sci.* **8** (1976) 99.
8. H.L. Tuller and A.S. Nowick, *J. Electrochem. Soc.* **126** (1979) 209.
9. P. Pascal, 'Nouveau Traité de Chimie minérale', Tome VII (Masson & Cie, Paris 1963).
10. G. Aguilar, L. Dupont, A. Foissy, J.P. Larpin and J.C. Colson, 'La Revue de Métallurgie-CIT/Science et Génie des Matériaux' (1993), p. 1607.
11. U. Lavrencic Stangar, B. Orel, I. Grabec, B. Ogorevec and K. Kalcher, *Solar Energy Mater. Sol. Cells* **316** (1993) 171.
12. F. Czerwinski, G.I. Sproule, M.J. Graham and W.W. Smeltzer, *Corros. Sci.* **37** (1995) 541.

13. C. Tanner, J.F. Jue and A.V. Virkar, *J. Electrochem. Soc.* **140** (1993) 1073.
14. C. Tanner and A.V. Virkar, *J. Am. Ceram. Soc.* **77** (1994) 2209.
15. S. Roure, F. Czerwinski and A. Petric, *Oxid. Met.* (*USA*) **42** (1994) 75.
16. M.F. Stroosnijder, V. Guttmann, T. Fransen and J.H.W. de Wit, *Oxid. Met.* (*USA*) **33** (1990) 371.
17. M. Cassir, V. Chauvaut, A. Alfarra and V. Albin, *J. Appl. Electrochem.* (2000) in press.
18. G. Moutiers, M. Cassir and J. Devynck, *J. Electroanal. Chem.* **324** (1992) 175.
19. M. Cassir, G. Moutiers and J. Devynck, *J. Electrochem. Soc.* **140** (1993) 3114.
20. B. Malinowska, M. Cassir, F. Delcorso and J. Devynck, *J. Electroanal. Chem.* **389** (1995) 21.
21. M. Cassir, M. Olivry, V. Albin, B. Malinowska and J. Devynck, *J. Electroanal. Chem.* **452** (1998) 127.
22. V. Chauvaut, M. Cassir and Y. Denos, *Electrochim. Acta* **43** (1998) 1991.
23. F. Culkin and J.P. Riley, *Anal. Chem.* **24** (1961) 167.
24. P. Burroughs, A. Hammett, A.F. Orchard and G. Thornton, *J. Chem. Soc., Dalton Trans.* (1976) 1686.
25. M. Romeo, K. Bak, J. El Fallah, F. Le Normand and L. Hilaire, *Surf. Interface Anal.* **20** (1993) 508.
26. A.E. Hughes, R.J. Taylor, B.R.W. Hinton and L. Wilson, *Surf. Interface Anal.* **23** (1995) 540.
27. E. Wuilloud, B. Deley, W.D. Schneider and Y. Baer, *Phys. Rev. Lett.* **53** (1984) 202.
28. M.P. Seah and W.A. Dench, *Surf. Interface Anal.* **1** (1979) 2.
29. J. Osterwalder, M. Sagurton, P.J. Orders, C.S. Fadley, B.D. Hermsmeir and D.J. Friedman, *J. Electron Spectros. Relat. Phenom.* **48** (1989) 55.
30. J.H. Scofield, *J. Electron Spectros. Relat. Phenom.* **8** (1976) 129.
31. G. Deroubaix and P. Marcus, *Surf. Interface Anal.* **18** (1992) 39.